

Article

# Occurrence of Sesquioxide in a Mid-Low Grade Collophane-Sedimentary Apatite Ore from Guizhou, China

Jie Deng <sup>1</sup>, Kecheng Zhang <sup>2</sup> , Dongsheng He <sup>2,\*</sup> , Hengqin Zhao <sup>3</sup>, Rachid Hakkou <sup>4</sup> and Mostafa Benzaazoua <sup>5,\*</sup> 

<sup>1</sup> Institute of Multipurpose Utilization of Mineral Resources, Chinese Academy of Geological Sciences, Chengdu 610041, China; dengjie23@126.com

<sup>2</sup> Xingfa School of Mining Engineering, Wuhan Institute of Technology, Wuhan 430073, China; zhangkecheng1996@163.com

<sup>3</sup> Institute of Multipurpose Utilization of Mineral Resources, Chinese Academy of Geological Sciences, Zhengzhou 450006, China; hengqin.z@126.com

<sup>4</sup> IMED-Lab, Sciences and Technics Faculty, Cadi Ayyad University (UCA), Marrakech BP 549/40000, Morocco; rhakkou@fstg-marrakech.ac.ma

<sup>5</sup> Reserach Institute in Mining and Environment, University of Quebec (RIME-UQAT), Rouyn-Noranda, QC J9X 5E4, Canada

\* Correspondence: hds@wit.edu.cn (D.H.); mostafa.benzaazoua@uqat.ca (M.B.)

Received: 11 October 2020; Accepted: 17 November 2020; Published: 20 November 2020



**Abstract:** Checking the presence of sesquioxide ( $\text{Fe}_2\text{O}_3$ ,  $\text{Al}_2\text{O}_3$ ) is helpful for its removal in advance. Therefore, the occurrence of sesquioxide in a mid-low grade calcareous-siliceous collophane ore (massive carbonate-apatite, also known as francolite) from Guizhou, China was determined by X-ray fluorescence spectroscopy (XRF), X-ray diffraction (XRD), field emission scanning electron microscope-energy dispersive X-ray spectrometry (FESEM-EDX) and Mineral Liberation Analyzer (MLA). The results show that iron mainly occurs as pyrite  $\text{FeS}_2$ , goethite  $\text{FeO}(\text{OH})$  and as substitution within dolomite  $\text{Ca}(\text{Mg},\text{Fe})(\text{CO}_3)_2$ , while aluminum is enriched in muscovite  $\text{KAl}_2(\text{AlSi}_3\text{O}_{10})(\text{OH})_2$  and also found in apatite  $(\text{F},\text{CO}_3)\text{CaPO}_4$  and calcite  $\text{CaCO}_3$  due to isomorphism or adsorption. All these minerals are fine-grained, among which pyrite and goethite tend to be enriched in larger particles. Intergrowth is predominant in the six minerals' locking. Pyrite is mainly intergrown with calcite, biotite and also included in apatite and muscovite, while the monomer pyrite appears as semi-automorphic fine grain with the liberation of 56.1%. Apatite particles are mainly intergrown with quartz and calcite. Most of goethite, dolomite, muscovite and calcite form intergrowth with apatite, with contents of 21.7%, 11.1%, 19.5% and 41%, respectively. The removal of pyrite, goethite, dolomite, muscovite and calcite in the ore is the key to reduce the contents of  $\text{Fe}_2\text{O}_3$  and  $\text{Al}_2\text{O}_3$ . In the subsequent beneficiation, the ore must be fully ground. In addition to flotation, magnetic separation can also be considered to remove part of iron in ore. For the removal of aluminum from apatite, leaching method can be considered.

**Keywords:** mid-low grade collophane ore; iron; aluminum; sesquioxide; occurrence

## 1. Introduction

Phosphate ore is an essential raw material for manufacturing phosphoric industrial products, which is nonrenewable, nonrecyclable and irreplaceable. The world's phosphate reserves in 2019 are 70 billion tons. Morocco has the largest phosphate reserves, which are 50 billion tons accounting for 71.43% of the total. China, Morocco, the United States and Russia are the leading phosphate

producing countries with a proportion of 79% [1]. According to mineralization, phosphate ore can be divided into three major types: igneous deposits, sedimentary deposits and biological deposits (guano accumulations). About 75% of phosphate resources are sedimentary [2].

The common gangue minerals (impurities) in phosphate rock include silicate minerals (quartz, mica), carbonate minerals (calcite, dolomite) and clay [3]. Most of phosphate rock in the world cannot be directly used in the production of phosphorus products, it must be through mineral processing to obtain economic utilization [4]. Due to the complex metallogenic environment, there are variable amounts of carbonates (calcite or dolomite) and silicates in sedimentary phosphate rock [5]. This makes it difficult to beneficiate from carbonate rich sedimentary phosphate deposits [6]. At present, phosphate ore processing can be different simple or complex combinations of the following processes: crushing, grinding, screening, scrubbing and desliming, heavy medium separation, washing, roasting, calcination and flotation [4,5]. Among these processes, flotation is the most widely used method and more than 60% of the commercial phosphate in the world is produced by flotation [2,7]. Before flotation, phosphate ores are usually subjected to other processes such as scrubbing and desliming, screening or classification. Scrubbing and desliming techniques are used to remove silicates (clays) [5]. Separating carbonate minerals from phosphates by flotation can be an ineffective process due to their similar physicochemical properties [5,8]. Calcination is an effective method to separate carbonate and phosphate minerals. During calcination, carbonates decompose to form free calcium and magnesium oxides, which can be removed by washing or slaking the thermally treated ore [9–11]. Tiit Kaljuvee et al. [12] studied the possibility of calcination-separation enrichment of carbonate-phosphorite ores from Karatau area. The content of  $P_2O_5$  in carbonate phosphate ores increased from 21–23% to more than 28% and the recovery of  $P_2O_5$  was not less than 85% by calcining phosphate ores in fluidized bed kiln, grinding the calcinated ores in a centrifugal impact mill and classifying the ground material in a non-rotary air separator. However, calcination is used for ores with low or average carbonate content and there are some problems in this method, such as low efficiency, high cost, excessive water consumption and extensive stages of grinding, washing, classification and so forth [5,12]. In view of the flotation separation of carbonate minerals in sedimentary phosphate ore, a lot of researches on flotation methods, flotation reagents, flotation influencing factors and mechanism have been carried out. For instance, using double reverse flotation [13,14], ultrasound irradiation-reverse flotation methods [8] to separate carbonates and phosphates; taking phosphoric acid ( $H_3PO_4$ ) [5] or citric acid ( $H_3Cit$ ) [15] as flotation depressant; developing new flotation collectors [16,17].

Phosphate ores also contain other metal impurities, such as iron, aluminum, titanium, manganese and even rare earth elements (such as La, Ce, Nd) in addition to the gangue minerals like silicates and carbonates [18]. The metal concentration in phosphate rock varies with origin, such that igneous rocks have lower concentrations whereas sedimentary rocks have higher concentrations [19]. Iron and aluminum are common impurity elements, which mainly exist in sedimentary phosphate ore as independent minerals and isomorphism. In nature, the major independent iron minerals include magnetite, hematite, limonite, pyrite, siderite and so forth, while aluminum minerals mainly involve diaspore, boehmite and gibbsite. These iron and aluminum minerals are often regarded as associated minerals of phosphate ores. Moreover, iron and aluminum can also be hosted in gangue minerals in the form of isomorphism, such as iron dolomite formed when  $Fe^{2+}$  is more than  $Mg^{2+}$ , fayalite, aluminosilicate minerals (like feldspar and mica). The contamination of iron emanating from limonite in phosphate concentrates has been a problem in phosphate ore flotation. The reason is that being similar floatability, limonite easily turns into flotation concentrates, then reducing the grade of concentrates. Therefore, increasing the surface hydrophilic of limonite to avoid the adhesion of air bubbles is one critical process in this separation process [20]. For high-iron phosphate ores, starch and its derivatives are usually used as depressant to depress the iron minerals in hematite based iron beneficiation [21,22]. However, flotation practice indicates that their separation effect is not ideal in the treatment of high-limonite phosphate ores with complex nature and fine dissemination [20]. Meanwhile, guar gum is extensively applied in the process of many oxides ores acting as depressant of iron oxide

minerals [23]. However, the high cost limits the application of guar gum in industrial flotation [24]. In view of this problem, Jun Yu et al. [20] studied the depression effect of sodium lignosulfonate on limonite in high iron collophane flotation, so as to improve the separation efficiency of collophane and limonite. The results showed that sodium lignosulfonate displayed a good depression effect toward limonite but had little depression effect on collophane flotation.

Iron and aluminum elements not only have an impact on phosphate ores beneficiation but also influence the subsequent phosphorus chemical production. Generally, the oxides of iron and aluminum are collectively referred to sesquioxides (expressed as  $R_2O_3$ ,  $Fe_2O_3 + Al_2O_3$ ) [25]. The sesquioxide makes difficult the production process of phosphoric acid and phosphate fertilizer and degrading the quality of products. When  $R_2O_3$  in phosphate ore is introduced into the system of phosphoric acid production, the consumption of sulfuric acid increases significantly, the growth of calcium sulfate crystal is interfered and phosphoric acid can be converted to sludge, resulting in a great loss of  $P_2O_5$ . In addition, iron and aluminum can form fine-crystal complexes with phosphate, which increases the viscosity of solution and slurry, easily blocks the pores of filter cloth and cake and also causes a difficulty to concentrate and dry phosphoric acid, which leads to undesirable quality of products [25,26]. Therefore, there are strict restrictions on the contents of iron and aluminum minerals in phosphate concentrate. For instance,  $Fe_2O_3/P_2O_5$  in concentrate is required to be less than 8% in the production of calcium superphosphate or phosphoric acid [27]. Thus, in order to obtain high-quality phosphate concentrate, the removal of sesquioxide from phosphate ore is necessary except the traditional de-magnesium and de-silicon, which requires more rational and effective beneficiation process and may increase the difficulty and cost of beneficiation.

Guizhou Province has abundant phosphate resources and the identified reserves rank the second in China [27]. Most of phosphate ore in Guizhou are marine sedimentary deposits, which is of various types, rich in small shelled animal fossils and algae and associated with other available resources such as rare earth elements, uranium [28–30]. Wu et al. [31] classified phosphate ore in Guizhou into 12 basic types through detailed study and investigation (Table 1). With the continuous depletion of phosphate ore, phosphate resources in the whole province are facing dilution problem. A great quantity of low-grade collophane (carbonate-rich fluorapatite) ore have become the main mining and utilization objects.

**Table 1.** Classification of phosphorite in Guizhou according to Wu et al. [31].

Texture Type		Ore Type	Origin	
Granular	Massive	Massive arenaceous phosphorite	Abnormal chemical conditions	
	Arenaceous	Laminated		Laminated arenaceous phosphorite
		Striped/banded		Striped/banded (dolomitic or clayey) arenaceous phosphorite
	Detrital			Gravel phosphorite
	Oolitic			Brecciated detrital phosphorite
	Coagulum			Oolitic phosphorite
	Agglomerate			Agglomerated arenaceous phosphorite
Gelatinous		Gel layered phosphorite	Authigene	
		Nodular phosphorite		
Biogenetic	Stromatolite	Cylindric stromatolite phosphorite	Biological	
	Algae	Algal arenaceous phosphorite		
	Shell	Bioclastic (containing small shell fossils) arenaceous phosphorite		

Checking the occurrence accurately and comprehensively is an important step in sesquioxide removal from colophane ore. This can provide theoretical basis for beneficiation process selection and optimization index control and is of great significance for the effective utilization of phosphate resources. However, most of the current works are about the removal of silicon and magnesium from Guizhou phosphate rock and the research on sesquioxide in Guizhou phosphate rock has not been done on industrial scale. In this study, X-ray fluorescence spectroscopy (XRF), X-ray diffraction (XRD), field emission scanning electron microscope-energy dispersive X-ray spectrometry (FESEM-EDX) and Mineral Liberation Analyzer (MLA) were used to characterize a colophane ore in Guizhou. Therefore, the main objective of this work is to determine the mineral species, particle size distribution and embedded characteristics of sesquioxide ( $R_2O_3$ ) in colophane.

## 2. Materials and Methods

### 2.1. Site Description

The sample for this study was collected from Kaiyang phosphate mining area located in Jinzhong Town, 86 km north of Guiyang City, Guizhou Province, 29 km away from Kaiyang County [32]. It starts from Wenquan Town in the north and ends at Yongshaba Town in the south. This mining area is famous for its large output and high grade (the average grade of  $P_2O_5$  is 33.32%) [33]. And it is composed of six sections, namely, Maluping, Niuganchong, Yongshaba, Jile, Liangchahe and Shabatu [34]. The potential in this area is high in the south and low in the north. The elevation of the highest point is 1713 m and the lowest point is at the junction of Yangshui river and Liangchahe river, with an elevation of 722 m. The basin terrain in the area is ridge valley with width of about 3–5 km. The ridges on both sides of the valley face each other. In the valley, the mountains are high and steep with relative elevation difference of 300–500 m and the gullies are developed, of which the density reaches 1.4 km/km<sup>2</sup>. The terrain gradient is steep, generally 30–50° [32]. Kaiyang phosphate deposit is located on the Yangshui anticline which is asymmetric and the axis of the anticline is 25° NE, the dip angle of the east side is 25–45° and the west side is 45–75°. The specific situation of Kaiyang phosphate mining area is shown in Figure 1 [33].

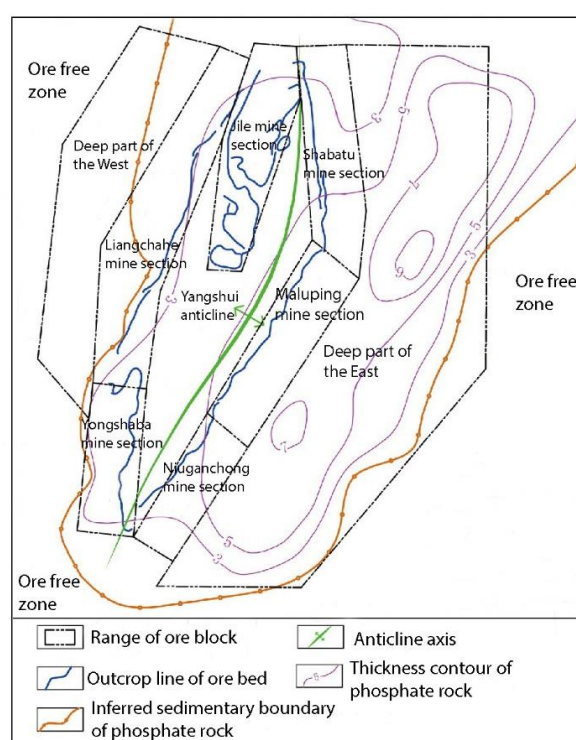


Figure 1. Map of Kaiyang phosphate mining area in Guizhou Province, China [33]

## 2.2. Sampling

The ore sample was collected from No. 3 ore heap and the sampling point was about 1 m away from the bottom of the ore heap. The colophane ore sample (about 500 kg) was first crushed to about 1 mm particle size by jaw crusher (model PEW760, Shanghai Shibang Machine (SBM) Group, Shanghai, China) -cone crusher (model HPC300-F2, Zhengzhou Great Wall Heavy Industry Machinery Co. Ltd., Zhengzhou, China) -roller mill (model MPG- $\phi$ 200  $\times$  75, Wuhan Exploring Machinery Factory, Wuhan, China). The samples within 1 mm particle size were divided by the sample splitter (model XSHF2-3, Wuhan Exploring Machinery Factory, China). The grinding of the divided subsamples was done in a laboratory bar mill (model HLXMB- $\phi$ 240  $\times$  300, Wuhan Hengle Mineral Engineering Machinery Co. Ltd., Wuhan, China) to ensure that the particle size of 90% of the subsamples was less than 0.075 mm and then a certain amount of representative samples were reduced. The ore sample for analysis was taken by spinning sample riffles (model XSHF2-3, Wuhan Exploring Machinery Factory, Wuhan, China) and dried put into for use.

## 2.3. Methods of Characterization

Semiquantitative analysis was performed by X-ray fluorescence (XRF) (model Bruker S4 PIONEER, Bruker Corporation, Mannheim, Germany) with a rhodium anode tube, to check the contents of major constituents and trace elements in the sample. The mineral phase composition was identified by X-ray diffraction (XRD) (model Bruker D8 ADVANCE, Bruker Corporation, Mannheim, Germany). The analysis conditions as following: starting and ending angles are  $3.000^\circ$  and  $70.008^\circ$  with a step in angle  $0.004^\circ$ , scanning rate of  $2.000^\circ$  and  $\text{CuK}\alpha 1$  radiation. A field emission scanning electron microscope (FESEM) equipped with an energy dispersive X-ray spectrometry (EDX) detector (model ZEISS GeminiSEM 300, Carl Zeiss AG, Jena, Germany) was used to determine the element distribution on the colophane ore surface. The accelerating voltage was 10 kV. Mineralogy was carried out with Mineral Liberation Analyzer (MLA). The MLA includes a FEI Quanta 650 SEM (FEI Company, Hillsboro, OR, USA) equipped with two Bruker Quantax 200 X-Flash 5010 EDX detectors (Bruker Corporation, Mannheim, Germany) and FEI's MLA Suite 3.1.4 for automated data acquisition. In order to analyze the loose solid material, it was mounted in an epoxy block and 3 g of the material were mixed with graphite and epoxy resin. Resulting sample block (30 mm in diameter) was ground and polished. The polished sample block was carbon coated using a Leica MED 020 vacuum evaporator (Leica, Wetzlar, Germany) to ensure conductivity of the sample surface.

## 3. Results

### 3.1. Properties of Collophane Ore

The chemical and mineralogical composition of the colophane ore are shown in Tables 2 and 3, Figure 2 gives the XRD phase analysis result of the colophane ore and Figure 3 shows the dissemination characteristics of some main mineral particles. The grade of  $\text{P}_2\text{O}_5$  is 25.94%, which accords with the characteristic of typical mid-low grade phosphate ore.  $\omega(\text{CaO})/\omega(\text{P}_2\text{O}_5)$  is about 1.48 ( $>1.4$ ) and the content of  $\text{SiO}_2$  is relatively high, which is 17.14%. All of these indicate that the sample is mid-low grade calcareous-siliceous colophane ore. The content of sesquioxide ( $\text{Fe}_2\text{O}_3$ ,  $\text{Al}_2\text{O}_3$ ) is 7.443%. It can be seen from Table 3 and Figure 2 that mineralogical composition of the ore is complex. Apatite as phosphate mineral is the main useful mineral with a content of 68.42%. Gangue minerals include silicate minerals (quartz, anorthite, muscovite, hornblende, etc.), carbonate minerals (calcite, dolomite) and other traces of orthoclase, kaolinite, pyrite, goethite, barite, biotite and so forth. Quartz, calcite and dolomite make up the most of gangue minerals. It can be seen from Figure 3 that most of apatite present in the shape of hypidiomorphic granular, dense block or strip structure, which is unevenly distributed in gangue minerals. It is also found that the larger apatite particle includes smaller irregular gangue minerals such as hornblende. In addition, some strip apatite and quartz form shell-like intergrowth. Pyrite is mainly scattered in the matrix in irregular granular or clastic granular structure and a small

amount of pyrite is embedded with apatite or other gangue minerals. Due to the low content of magnesium in ore, the main task of flotation is to remove silicon and sesquioxide.

**Table 2.** Chemical composition of Guizhou collophane ore.

Component	Content (wt.%)	Component	Content (wt.%)
P <sub>2</sub> O <sub>5</sub>	25.94	SO <sub>3</sub>	1.56
CaO	38.45	TiO <sub>2</sub>	0.269
MgO	1.96	MnO	0.0825
SiO <sub>2</sub>	17.14	CuO	0.0215
Fe <sub>2</sub> O <sub>3</sub>	1.283	ZnO	0.0395
Al <sub>2</sub> O <sub>3</sub>	6.16	Rb <sub>2</sub> O	0.001
Na <sub>2</sub> O	0.203	SrO	0.083
K <sub>2</sub> O	1.41	ZrO <sub>2</sub>	0.0113
F	2.54	BaO	0.498
Cl	0.015		

**Table 3.** Mineralogical composition of Guizhou collophane ore.

Mineral	Content (wt.%)	Mineral	Content (wt.%)
Apatite	68.42	Barite	0.24
Orthoclase	0.29	Muscovite	2.51
Quartz	8.41	Rutile	0.06
Kaolinite	0.47	Biotite	0.42
Anorthite	2.87	Diopside	0.04
Pyrite	0.99	Native iron	0.02
Hornblende	1.77	Enargite	0.02
Calcite	8.32	Fayalite	0.07
Goethite	0.28	BaSiO <sub>3</sub>	0.01
Chlorite	0.02	(Ca, Fe) silicate	0.04
Augite	0.05	Apatite + Pyrite	0.07
Albite	0.06	V spinel	0.01
Dolomite	4.55	In total	100.00

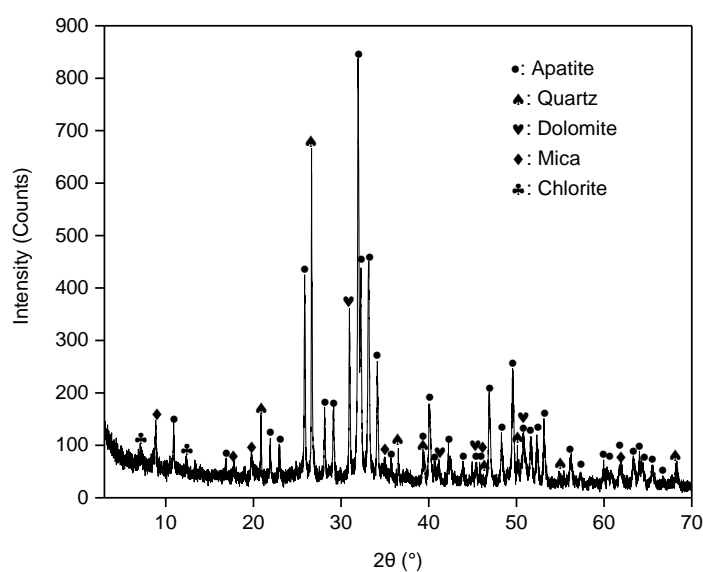


**Figure 2.** X-ray diffraction (XRD) phase analysis of Guizhou collophane ore.

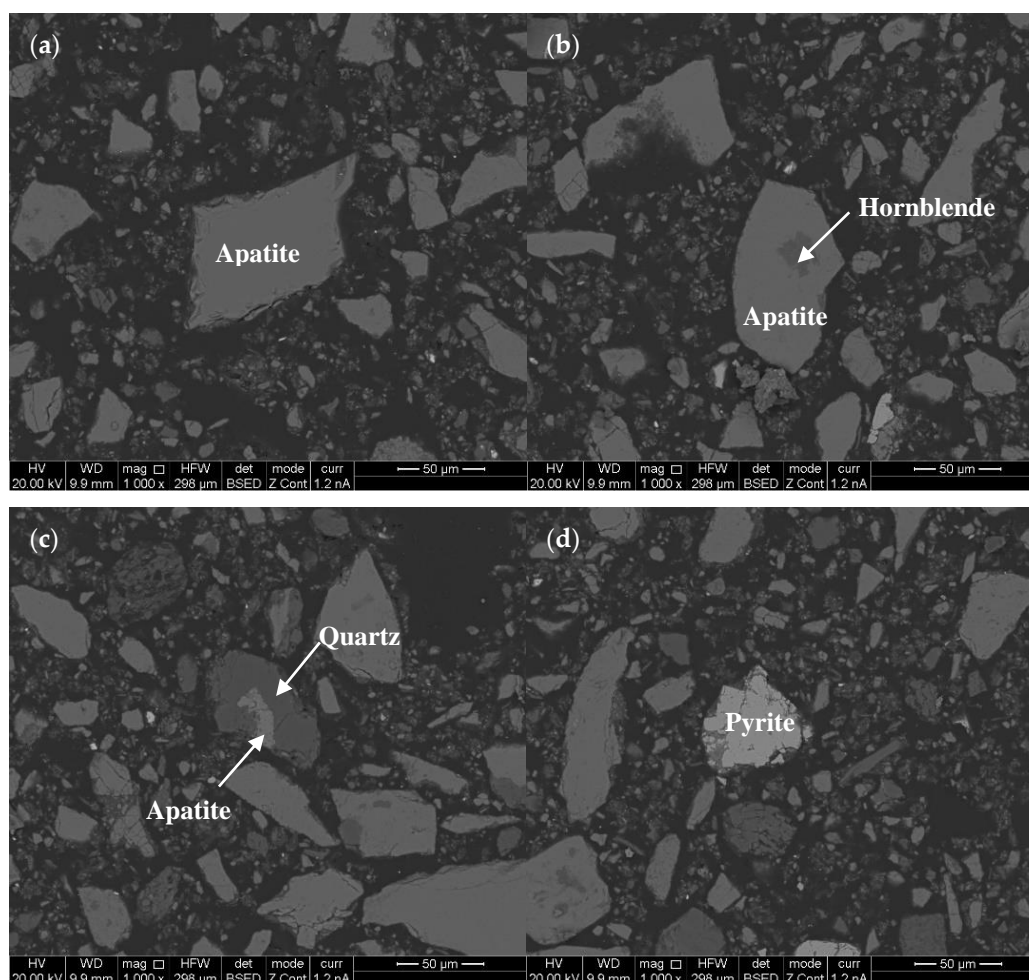


**Figure 3.** Dissemination characteristics of main mineral particles: (a) Apatite mineral; (b) Hornblende was included by apatite; (c) Apatite was included by quartz; (d) Pyrite mineral.

### 3.2. Distribution of Fe and Al in Collophane Ore

The distribution of Fe and Al in collophane ore are given in Tables 4 and 5. The EDX mapping analysis of collophane ore and pyrite is shown in Figures 4–7. Fe and Al are basically found in gangue minerals. Fe is relatively enriched in pyrite  $\text{FeS}_2$  and goethite  $\text{FeO}(\text{OH})$  as independent minerals and also hosted in dolomite  $\text{Ca}(\text{Mg}, \text{Fe})(\text{CO}_3)_2$  in the form of isomorphism, having proportions of 50.1%, 13.9% and 16%, respectively. Al mainly occurs as a component element within muscovite  $\text{KAl}_2(\text{AlSi}_3\text{O}_{10})(\text{OH})_2$  and is also found in apatite and calcite in the form of isomorphism or adsorption, which account for 24.9%, 19.7% and 19.1%, respectively. The EDX elements mapping results of collophane ore show that the distribution of Fe, S, Mg and Ca is consistent, especially Fe and S, which indicates that Fe exists in pyrite and dolomite as  $\text{FeS}_2$  or  $\text{Ca}(\text{Mg}, \text{Fe})(\text{CO}_3)_2$ ; Si and Al have the same distribution characteristics, indicating that most of Al elements are held in silicate minerals. Further analysis of EDX elements mapping and spectrum of pyrite shows that in addition to the main elements S and Fe, there are also a small amount of Si, Al, Ca, Mg, P elements in the pyrite particles, which indicates that some pyrite particles are mixed with a small amount of aluminosilicate minerals and apatite.

**Table 4.** Distribution of Fe in colophane ore determined by Mineral Liberation Analyzer (MLA) \*.

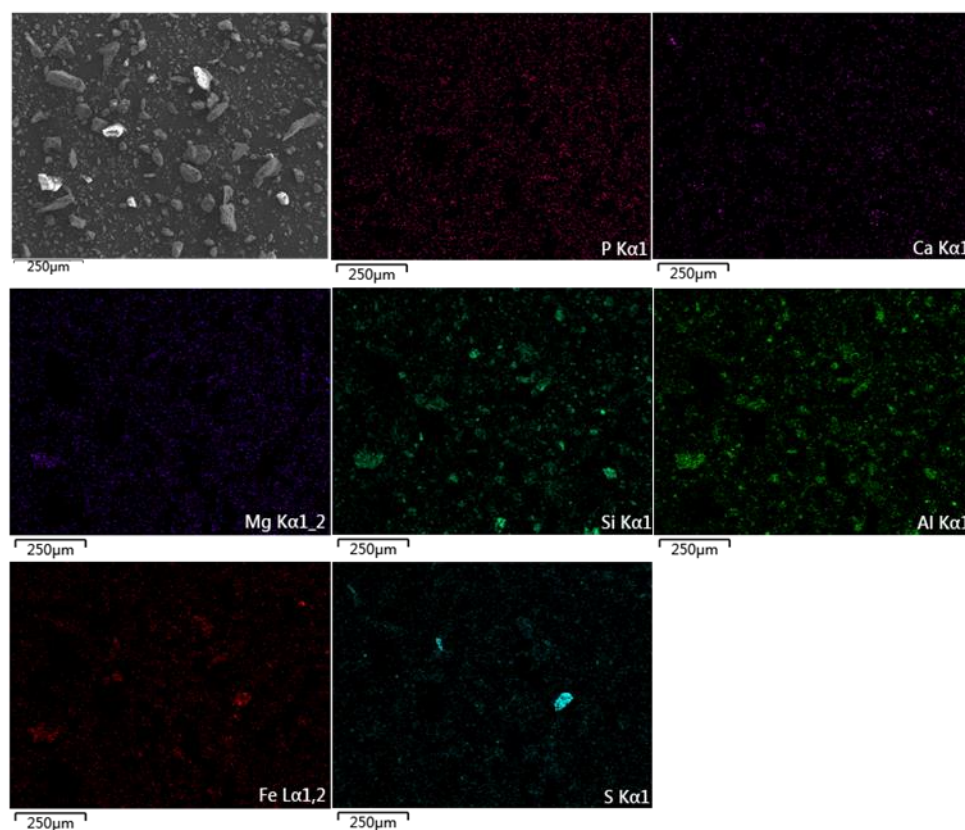
Mineral	Content (wt.%)	Mineral	Content (wt.%)
Kaolinite	1.40	Dolomite	16.00
Anorthite	5.56	Biotite	2.79
Pyrite	50.12	Native iron	1.67
Hornblende	2.55	Fayalite	1.44
Goethite	13.89	(Ca, Fe) silicate	1.00

\*: Only minerals with more iron and aluminum are listed, which does not mean that the remaining minerals do not contain iron and aluminum.

**Table 5.** Distribution of Al in colophane ore determined by MLA \*.

Mineral	Content (wt.%)	Mineral	Content (wt.%)
Apatite	19.65	Hornblende	2.67
Orthoclase	1.92	Calcite	19.09
Quartz	6.76	Muscovite	24.90
Kaolinite	5.23	Biotite	3.33
Anorthite	14.77	Albite	0.46

\*: As in Table 4, only minerals with more iron and aluminum are listed, which does not mean that the remaining minerals do not contain iron and aluminum.

**Figure 4.** Energy dispersive X-ray spectrometry (EDX) elements mapping of colophane ore.

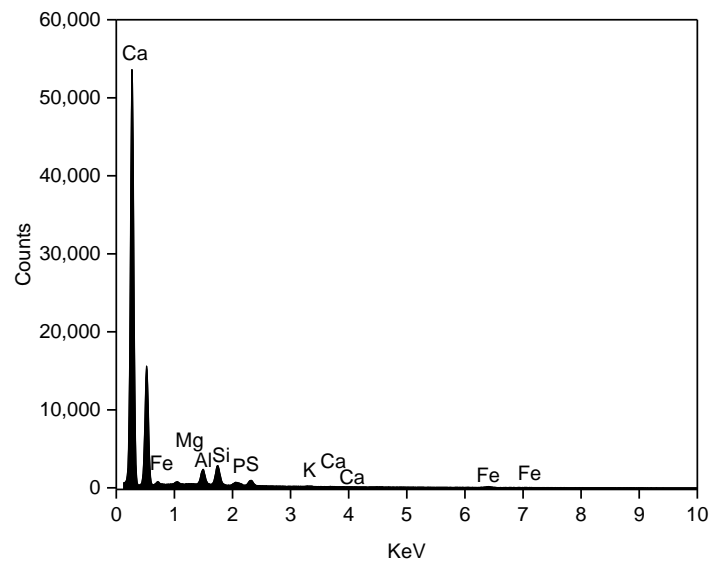


Figure 5. EDX spectra of collophane ore.

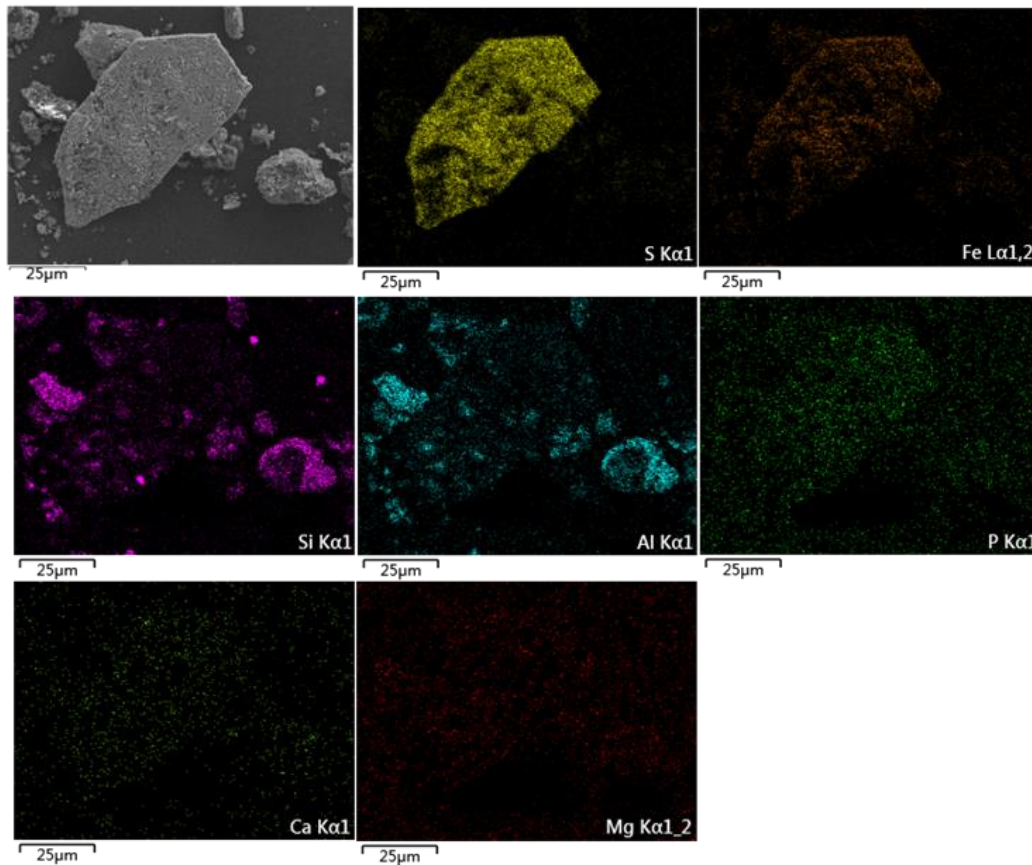
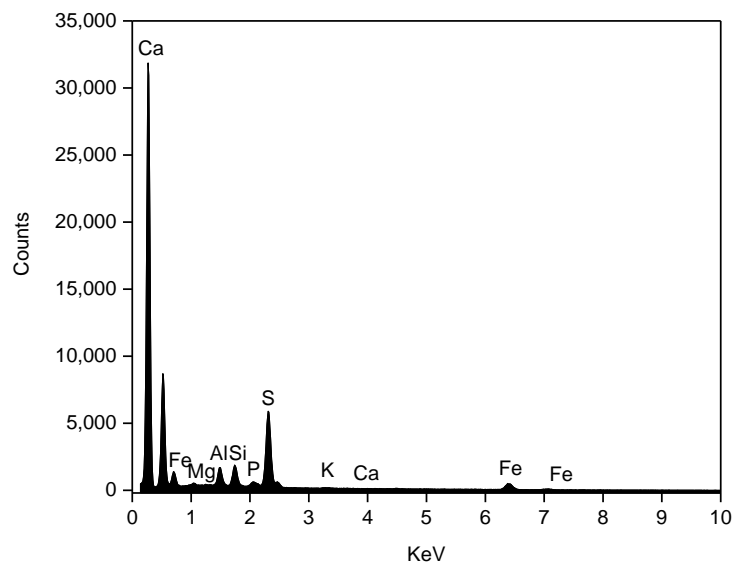


Figure 6. EDX elements mapping of pyrite.



**Figure 7.** EDX spectra of pyrite.

### 3.3. Grain Size Distribution of Main Fe, Al-Bearing Minerals

Checking the particle size of minerals is helpful to guide the crushing and grinding stages in mineral processing. When the mineral particles are fine and closely associated with each other, it may be regarded as a whole in the beneficiation operation, thus the ore must be fully crushed before it can be dissociated. In addition, the mineral particle size has an effect on the flotation process. Flotation requires not only sufficient liberation of minerals but also suitable particle size. If the ore particle is too coarse, exceeding the floating load capacity of the bubble, it will not float; if the ore particle is too fine, it is unfavorable to flotation. In order to figure out main Fe-bearing (pyrite, goethite, dolomite) and Al-bearing (apatite, muscovite, calcite) minerals distribution in different particle sizes, particle size analysis of several minerals was carried out. The results are shown in Figure 8. Pyrite, goethite and dolomite are all fine-grained with grain sizes within 75  $\mu\text{m}$ . Among the three minerals, both of pyrite and goethite tend to be enriched in larger particles. When the sieve sizes of pyrite, goethite and dolomite are 53–63  $\mu\text{m}$ , 27–32  $\mu\text{m}$  and 38–45  $\mu\text{m}$ , the mass fraction on sieve reaches the maximum, which are 16.3%, 15.6% and 11.6% respectively. The three minerals are mainly concentrated in 16–75  $\mu\text{m}$ , 8.1–32  $\mu\text{m}$  and 8.1–45  $\mu\text{m}$ , accounting for 72.8%, 79.9% and 85.1% of the total respectively.

It can be seen from Figure 8 that the grain sizes of apatite, muscovite and calcite are also relatively small, which in the order of apatite > muscovite > calcite. When the sieve sizes of apatite, muscovite and calcite are 38–45  $\mu\text{m}$ , 11.4–13.5  $\mu\text{m}$  and 8.1–9.6  $\mu\text{m}$ , the mass fraction on sieve is the largest, which are 9.1%, 12.8% and 26.1% respectively. The three minerals are enriched in 22–75  $\mu\text{m}$ , 8.1–32  $\mu\text{m}$  and 6.8–11.4  $\mu\text{m}$ , which account for 60%, 77.1% and 58.4% of the total respectively. Since there are many fine particles in these single minerals, the grinding size must be fine enough to separate them from the useful mineral as much as possible.

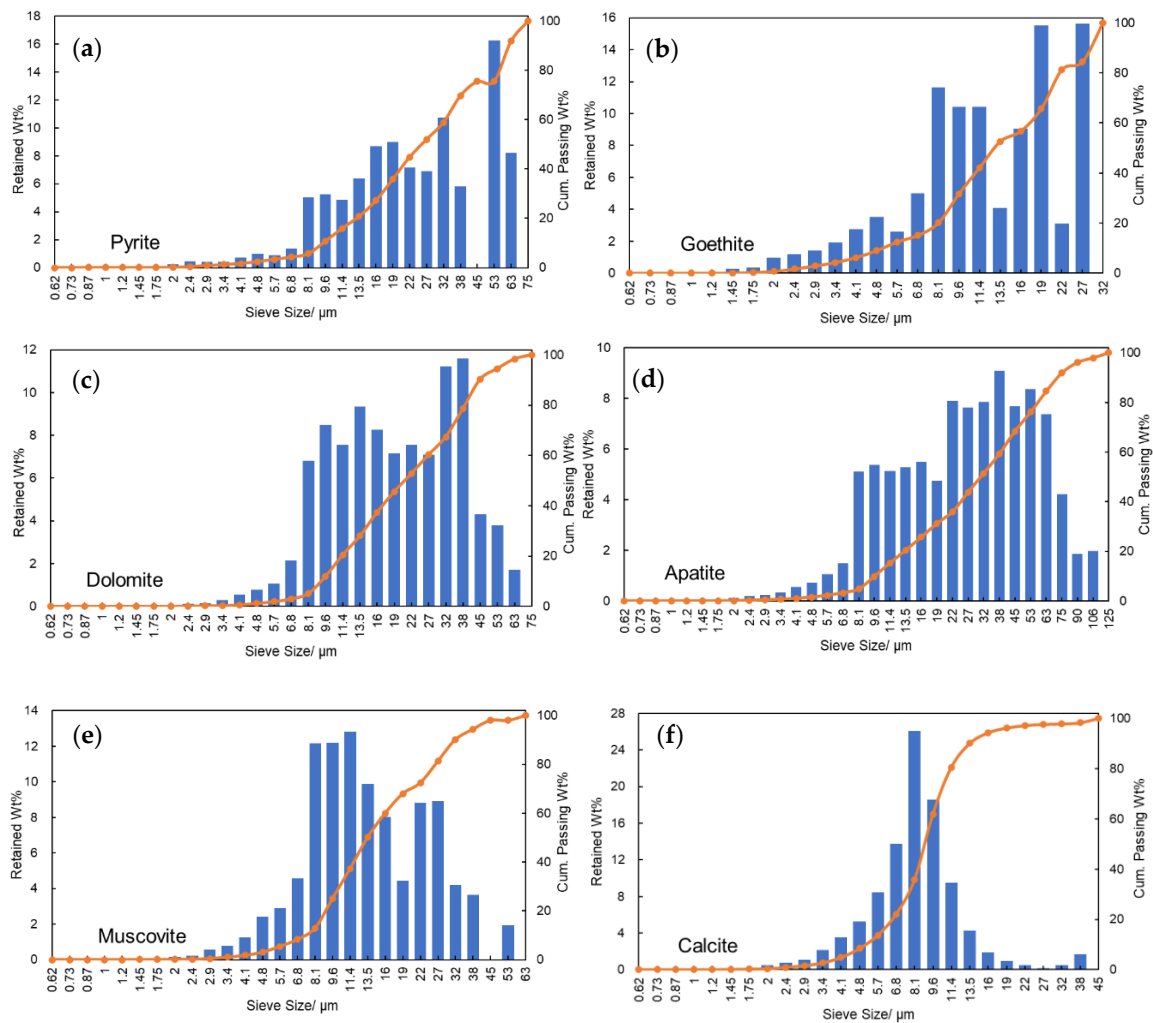


**Figure 8.** Grain size distribution of Fe, Al-bearing minerals: (a) pyrite; (b) goethite; (c) dolomite; (d) apatite; (e) muscovite; (f) calcite.

### 3.4. The Association between Main Fe, Al-Bearing Minerals and Other Minerals

The liberations of pyrite, goethite, dolomite, apatite, muscovite and calcite and their association with other minerals were determined by MLA. The results are given in Figures 9–11. In the figure, binary and tertiary or greater mean that the mineral studied is intergrown with and included by other minerals.

Pyrite is mainly intergrown with calcite, biotite, with contents of 5.1% and 5.4% respectively. The proportion of pyrite included in muscovite and apatite is also relatively large, which is 3.4% and 2.7% respectively (Figure 9a). According to Figure 9b, most of goethite forms intergrowth with apatite, with a content of 21.7%, followed by 8.4% of goethite with (Ca, Fe) silicate. From Figure 9c, it shows that dolomite is associated with apatite and calcite in a larger proportion, especially apatite, with a prominent proportion of 11.1%.

According to Figure 10a, apatite is mainly intergrown with quartz and calcite, with contents of 6.7% and 8.4% respectively. From Figure 10b, it shows that muscovite mainly forms intergrowth with apatite, the content of which is 19.5% and according to Figure 10c, the proportion of calcite intergrown with apatite is significant, which is 41%.

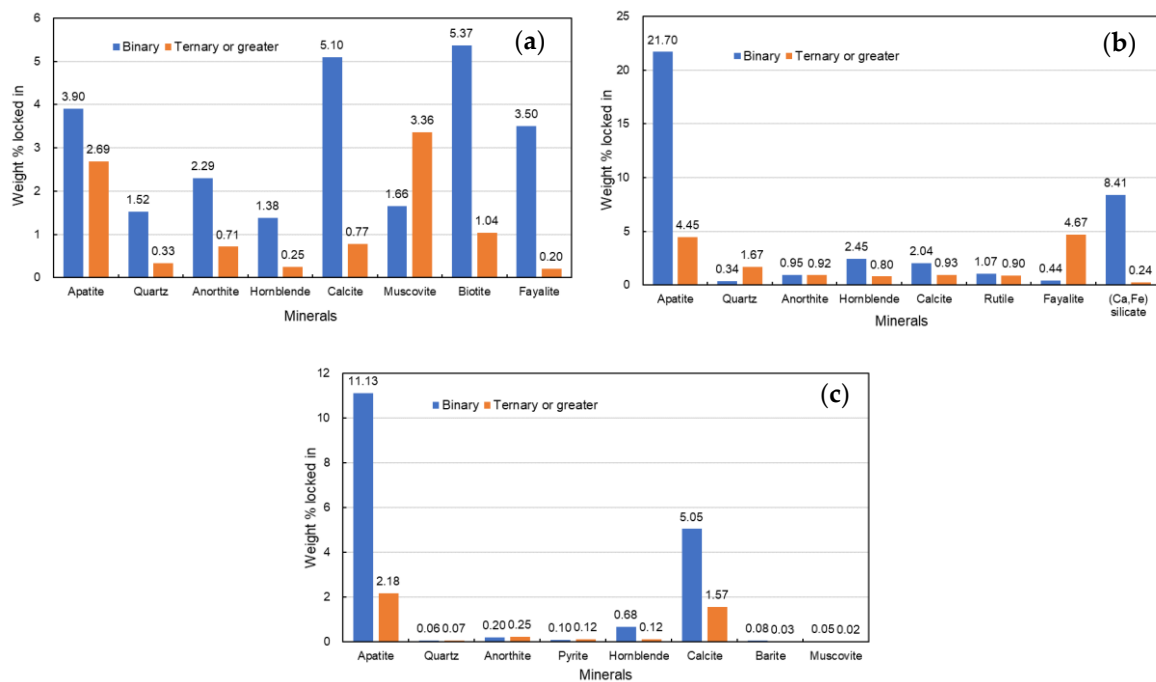


**Figure 9.** Intergrowth and inclusion contents between the Fe-bearing minerals and other minerals measured by MLA: (a) Pyrite; (b) Goethite; (c) Dolomite.

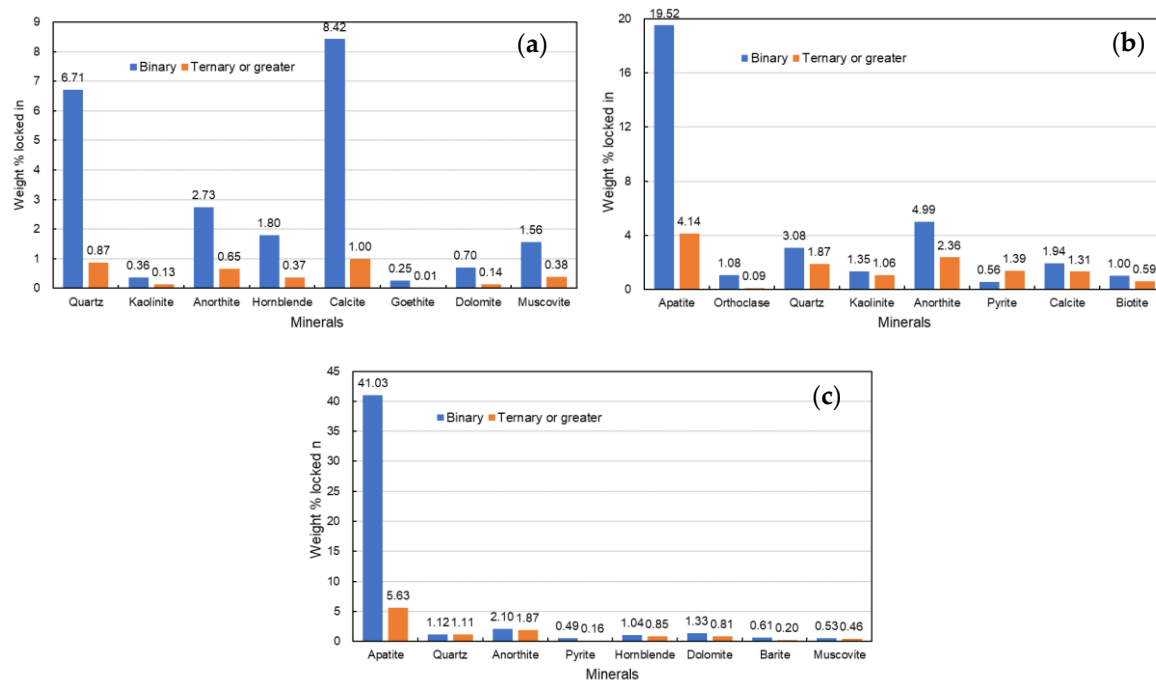


**Figure 10.** Intergrowth and inclusion contents between the Al-bearing minerals and other minerals measured by MLA: (a) Apatite; (b) Muscovite; (c) Calcite.

The purpose of ore separation is to effectively enrich and recover useful minerals and the liberation of minerals within the optional particle size range will directly affect the separation effect. Therefore, accurate prediction and determination of the liberation of iron and aluminum bearing minerals will further improve the beneficiation effect of colophane ore. In Figure 11, it can be seen that except for the liberation, intergrowth is predominant in the six minerals' locking. Among them, calcite has the largest intergrown proportion, accounting for 48.2%, which is also the reason for the lowest liberation of calcite

mineral. Moreover, the content of liberated goethite is also less, which indicates that grinding can only separate a small part of goethite from the ore and the majority must be removed by other means. The contents of liberated apatite and dolomite are relatively high in all the six minerals, which are 73.4% and 78% respectively. Combining Figures 9 and 10, it can be concluded that most of pyrite can be removed from grinding and flotation together with calcite and muscovite that contain aluminum. Although fine-grained goethite, dolomite, muscovite and calcite are slightly different in intergrown and included content with other minerals, they are mainly closely intergrown with apatite, which means that it is difficult to remove Fe and Al from colophane ore and the separation cost is high.

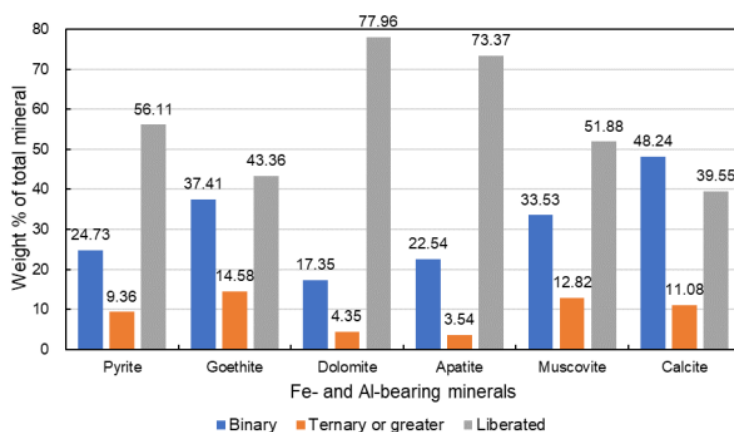


**Figure 11.** The total contents of each of the six minerals in the state of monomer liberation, intergrowth and inclusion.

#### 4. Discussion

Obviously, the removal of pyrite, goethite, dolomite, muscovite and calcite in the ore is the key to reduce the contents of  $\text{Fe}_2\text{O}_3$  and  $\text{Al}_2\text{O}_3$ .

Pyrite is an abundant mineral in nature with a chemical formula of  $\text{FeS}_2$ . It is usually associated with other sulfides (such as sulfide ores containing galena) and oxides [35,36]. Pyrite is rich in the earth's surface and has been found in the composition of sedimentary and metamorphic rocks, in coal beds and as an alternative mineral in fossils [35]. Sedimentary pyrite generally forms by the reaction of detrital iron minerals with  $\text{H}_2\text{S}$  during the stage of shallow burial [37,38]. Under anoxic conditions, seawater sulfate is reduced to  $\text{H}_2\text{S}$  by bacteria, which reacts with detrital iron minerals and forms pyrite [39–41]. In modern sediments as well as in ancient Phanerozoic, Proterozoic and Archean sedimentary rocks, the dominant textural forms of pyrite are euhedral crystals and framboids [42,43]. Pyrite framboids are dense spherical aggregates, composed of submicron-sized pyrite crystals [43]. There are high crystallinity pyrites in the United States, Peru, China and Spain [35].

As an important mineral, pyrite can be used as a precursor of products, such as sulfur, sulfuric acid, hematite, sulfur dioxide, fertilizers and ferrous sulfate [35]. It has also been widely used in the preparation of smoke agents, rubber, paper, textiles, matches, cathodes for lithium batteries especially for semiconductor materials in the chemical industry [44–47]. Pyrite oxidation produces sulfuric acid and iron oxyhydroxides [48]. When Peter Kraal et al [48]. investigated the phosphorus (P) and iron (Fe) fractionation in anoxic sediments, it was found that iron-bound phosphorus accounted for up to 99% of total phosphorus in carbonate-poor samples and its abundance was related to pyrite contents. The phosphorus fractionation in anoxic, carbonate-poor sediments is strongly affected by pyrite oxidation. Pyrite oxidation leads to a conversion of authigenic calcium-phosphorus to iron-bound phosphorus. In more calcareous samples,  $\text{CaCO}_3$  can act as an effective buffer against acidic dissolution of Ca–P minerals.

Goethite ( $\alpha\text{-FeOOH}$ ) is a naturally occurring iron oxy-hydroxide mineral, which is a ubiquitous phase in many iron ore types and found in association with several types of mineral deposits including

iron, manganese and bauxite ores. It is typically the weathering product of iron-bearing minerals formed through inorganic chemical or organic precipitation under oxidation conditions. It has different shapes, sizes and morphology. Goethite is basically composed of Fe, O and OH, distinguished and named according to the differences of the water content. Due to its large surface area and typical structural arrangement (tunnel type), it has a large water absorption capacity. Goethite may contain variable amounts of impurities, such as  $\text{Al}_2\text{O}_3$ , MnO, CaO and  $\text{SiO}_2$ , which sometimes up to 5% [49]. Goethite processing is difficult because it contains many harmful impurities and it is also the main component of many iron ore plant reject streams [50]. Depending on temperature and reduction conditions, goethite can be transformed to hematite, magnetite and other minerals suitable for magnetic separation [50]. Therefore, there are many studies on the treatment of goethite by reduction roasting followed by magnetic separation [50–53]. Sometimes, goethite contains a high content of phosphorus (P) and the existing phosphorus removal techniques is to thermally roasted the ore with or without alkaline additives followed by chemical or water leaching [54–57]. However, up to date, none of these proposed dephosphorization routes for goethite have been commercialized and current method of utilizing goethite ore in steelmaking remains to be blending with other low-P ore to balance out the overall phosphorus input to the blast furnace [58,59]. Therefore, bio-beneficiation dephosphorization of goethite ore has been studied as a relatively new approach [58]. Williams et al. [60] used some sulfide-oxidizing bacteria to reduce the pH value to  $\leq 1$ , in which apatite can selectively dissolve.

Muscovite [ $\text{K}_2\text{Al}_4(\text{Si}_6\text{Al}_2\text{O}_{20}(\text{OH},\text{F})_4$ ] is typically formed by metamorphism of impure limestones and igneous rocks. It is a 2:1 layered phyllosilicate with an octahedral "O" layer sandwiched between two inward pointing tetrahedral "T" layers, forming "T-O-T" units. Muscovite usually exists in many ores as main gangue components [61,62]. It has a wide range of uses. Sheet mica is traditionally used as an electrical insulation material (such as mica paper), filler in the production of various putties, grout and paints and so forth. In addition, ultrafine muscovite can also be used to produce decorative coatings and cosmetics. The enrichment of muscovite-bearing materials can be carried out by traditional methods, such as gravity (spiral separation, concentration on tables), magnetic separation and flotation [63].

In apatite, the ability of anion to replace phosphate is not limited to  $\text{F}^-$ ,  $\text{CO}_3^{2-}$  and  $\text{OH}^-$ , which exist in different variants of apatite. Silicate, vanadate, aluminate, titanate and arsenate may also occur replacing part of phosphates. The extent to which substitution happen and what the substitute is depend on the prevailing conditions during the formation of apatite and on the effect of subsequent events (such as weathering). In marine sedimentary deposits, phosphates occur in mixtures with detrital materials such as quartz, mica and clay, often with limestone and occasionally with dolomite [4]. For the impurity aluminum in apatite, different elements in the same mineral are difficult to be separated by flotation, so the leaching method can be considered. Dolomite ( $\text{CaMg}(\text{CO}_3)_2$ ) and calcite ( $\text{CaCO}_3$ ) are common gangue minerals in sedimentary phosphate ores. Fe substitution often occurs in dolomite. Due to the similar surface properties of dolomite, calcite and apatite, the flotation separation can be a difficult process. However, in this paper, calcite is closely associated with pyrite, so it may be removed along with pyrite to a large extent.

## 5. Conclusions

After the samples was analyzed by XRD, XRF, FESEM-EDX and MLA, the following conclusions can be drawn:

The collophane ore studied in this paper is mid-low grade calcareous-siliceous, in which apatite is the main useful mineral and quartz, dolomite and calcite make up the most of gangue minerals. The content of sesquioxide ( $\text{Fe}_2\text{O}_3$ ,  $\text{Al}_2\text{O}_3$ ) in the ore is 7.443%. Iron is relatively enriched in pyrite  $\text{FeS}_2$  and goethite  $\text{FeO}(\text{OH})$  as independent minerals and also occurs as substitution within dolomite  $\text{Ca}(\text{Mg}, \text{Fe})(\text{CO}_3)_2$ . Aluminum is mostly hosted in muscovite  $\text{KAl}_2(\text{AlSi}_3\text{O}_{10})(\text{OH})_2$  and also found in apatite and calcite in the form of isomorphism or adsorption. The six minerals are all fine-grained, among which pyrite and goethite have similar content changes at different grain sizes and both of

them tend to be enriched in larger particles. Pyrite is mainly intergrown with calcite and biotite and also included in muscovite and apatite with a large proportion. The other four minerals (goethite, dolomite, muscovite and calcite) mostly form intergrowth with apatite. Apatite is mainly intergrown with quartz and calcite. Among the six minerals, the liberations of apatite and dolomite are higher, while the liberated calcite and goethite are less.

The removal of pyrite, goethite, dolomite, muscovite and calcite in the ore is the key to reduce the contents of  $\text{Fe}_2\text{O}_3$  and  $\text{Al}_2\text{O}_3$ . In the subsequent beneficiation, the ore must be fully ground. Most of pyrite can be removed from beneficiation together with calcite and muscovite that contain aluminum and magnetic separation can also be considered to remove part of iron in the ore except flotation. Goethite, dolomite, muscovite and calcite are closely intergrown with apatite in fine grain size, therefore, they are difficult to be separated during beneficiation and the separation cost is high. Since different elements in the same mineral are difficult to separate by flotation, leaching can be considered to remove aluminum from apatite.

**Author Contributions:** Conceptualization, D.H.; Formal analysis, J.D. and H.Z.; Methodology, J.D. and H.Z.; Writing—original draft, K.Z.; Writing—review & editing, R.H. and M.B. All authors have read and agreed to the published version of the manuscript.

**Funding:** This work was funded by Hubei Tailings (Slag) Resource Utilization Engineering Technology Research Center Project (No. 2019ZYD070), China Geological Survey Project (DD20190626), National Key Research and Development projects (2019YFC1905801).

**Conflicts of Interest:** The authors declare no conflict of interest.

## References

1. U.S. Geological Survey. *Mineral Commodity Summaries*; U.S. Geological Survey: Reston, VA, USA, 2019; pp. 122–123.
2. Abouzeid, A.-Z.M. Physical and thermal treatment of phosphate ores—An overview. *Int. J. Min. Process.* **2008**, *85*, 59–84. [[CrossRef](#)]
3. Özer, A.K.; Gülaboglu, M.; Bayrakcükken, S. Physical structure and chemical and mineralogical composition of the Mazidagi (Turkey) phosphate rock. *Ind. Eng. Chem. Res.* **2000**, *39*, 679–683. [[CrossRef](#)]
4. Aydin, I.; Imamoglu, S.; Aydin, F.; Saydut, A.; Hamamci, C. Determination of mineral phosphate species in sedimentary phosphate rock in Mardin, SE Anatolia, Turkey by sequential extraction. *Microchem. J.* **2009**, *91*, 63–69. [[CrossRef](#)]
5. Mohammadkhani, M.; Noaparast, M.; Shafaei, S.Z.; Amini, A.; Amini, E.; Abdollahi, H. Double reverse flotation of a very low grade sedimentary phosphate rock, rich in carbonate and silicate. *Int. J. Miner. Process.* **2011**, *100*, 157–165. [[CrossRef](#)]
6. Al-Fariss, T.F.; Ozbelge, H.O.; Abdulrazik, A.M. Flotation of a carbonate rich sedimentary phosphate rock. *Fert. Res.* **1991**, *29*, 203–208. [[CrossRef](#)]
7. Nunes, A.P.L.; Peres, A.E.C.; Chaves, A.P.; Ferreira, W.R. Effect of alkyl chain length of amines on fluorapatite and aluminium phosphates floatabilities. *J. Mater. Res. Technol.* **2019**, *8*, 3623–3634. [[CrossRef](#)]
8. Hassani, F.; Noaparast, M.; Tonkaboni, S.Z.S. A study on the effect of ultrasound irradiation as pretreatment method on flotation of sedimentary phosphate rock with carbonate–silicate gangue. *Iran. J. Sci. Technol. Trans. Sci.* **2019**, *43*, 2787–2798. [[CrossRef](#)]
9. Abouzeid, A.-Z.M.; El-Jallad, I.S.; Orphy, M.K. Calcareous phosphates and their calcined products. *Miner. Sci. Eng.* **1980**, *12*, 73–83.
10. Kumar, D. Calcination of phosphate rocks. *Chem. Eng. Technol.* **1980**, *52*, 736–740. [[CrossRef](#)]
11. Yousef, A.A.; El-Nozahi, S.M.; Ali, N. Some aspects on the beneficiation of Sebaiya phosphates, Egypt. *Erzmetall* **1982**, *35*, 428–431.
12. Kaljuvee, T.; Kuusik, R.; Veiderma, M. Enrichment of carbonate-phosphate ores by calcination and air separation. *Int. J. Miner. Process.* **1995**, *43*, 113–121. [[CrossRef](#)]
13. Amirech, A.; Bouhenguel, M.; Kouachi, S. Two-stage reverse flotation process for removal of carbonates and silicates from phosphate ore using anionic and cationic collectors. *Arab. J. Geosci* **2018**, *11*, 593. [[CrossRef](#)]

14. Ge, Y.Y.; Gan, S.P.; Zeng, X.P.; Yu, Y.F. Double reverse flotation process of collophanite and regulating froth action. *Trans. Nonferr. Met. Soc. China* **2008**, *18*, 449–453. [[CrossRef](#)]
15. Liu, X.; Luo, H.H.; Cheng, R.J.; Li, C.X.; Zhang, J.H. Effect of citric acid and flotation performance of combined depressant on collophanite ore. *Miner. Eng.* **2017**, *109*, 162–168. [[CrossRef](#)]
16. Huang, Z.; Cheng, C.; Liu, Z.; Zeng, H.; Feng, B.; Zhong, H.; Luo, W.; Hu, Y.; Guo, Z.; He, G.; et al. Utilization of a new Gemini surfactant as the collector for the reverse froth flotation of phosphate ore in sustainable production of phosphate fertilizer. *J. Clean. Prod.* **2019**, *221*, 108–112. [[CrossRef](#)]
17. Shao, X.; Jiang, C.L.; Parekh, B.K. Enhanced flotation separation of phosphate and dolomite using a new amphoteric collector. *Min. Met. Explor.* **1998**, *15*, 11–14. [[CrossRef](#)]
18. Aydin, I.; Aydin, F.; Saydut, A.; Bakirdere, E.G.; Hamamci, C. Hazardous metal geochemistry of sedimentary phosphate rock used for fertilizer (Mazıdag, SE Anatolia, Turkey). *Microchem. J.* **2010**, *96*, 247–251. [[CrossRef](#)]
19. Nziguheba, G.; Smolders, E. Inputs of trace elements in agricultural soils via phosphate fertilizers in European countries. *Sci. Total Environ.* **2008**, *390*, 53–57. [[CrossRef](#)]
20. Yu, J.; Ge, Y.Y.; Guo, W.B.; Guo, X.L. Flotation collophane from high-iron phosphate ore by using sodium ligninsulfonate as depressant. *Sep. Sci. Technol.* **2016**, 03–47. [[CrossRef](#)]
21. Nanthakumar, B.; Grimm, D.; Pawlik, M. Anionic flotation of high-iron phosphate ores—Control of process water chemistry and depression of iron minerals by starch and guar gum. *Int. J. Miner. Process.* **2009**, *92*, 49–57. [[CrossRef](#)]
22. Yu, K.P.; Yu, Y.F.; Xu, X.Y. Separation behavior and mechanism of hematite and collophane in the presence of collector RFP-138. *Trans. Nonferr. Met. Soc. China* **2013**, *23*, 501–507. [[CrossRef](#)]
23. Guimaraes, R.; Araujo, A.C.D.; Peres, A. Reagents in igneous phosphate ores flotation. *Min. Eng.* **2005**, *18*, 109–204. [[CrossRef](#)]
24. Zhao, K.; Gu, G.; Wang, C.; Rao, X.; Wang, X.; Xiong, X. The effect of a new polysaccharide on the depression of talc and the flotation of a nickel-copper sulfide ore. *Miner. Eng.* **2015**, *77*, 99–106. [[CrossRef](#)]
25. He, B.B.; Zhang, H.; Fu, Y.; Zhou, Q.B.; Zhao, Z.B.; Peng, Q.S. Feasibility research on reducing sesquioxide content of phosphate and phosphoric acid. *Phosphate Compd. Fertil.* **2016**, *31*, 37–38. [[CrossRef](#)]
26. Li, X.; Zhu, G.Y.; Gong, X.K.; Li, S.P.; Xu, W.; Li, H.Q. Occurrence of the Impurities in Phosphorus Rock and the Research of Acidolysis Process. *Spectrosc. Spectr. Anal.* **2019**, *39*, 1288–1293. [[CrossRef](#)]
27. Chen, G.; Zhang, T.; Zhao, W.Q.; Zhang, W.S.; Chen, K.X. Research progress of de iron and de aluminum of phosphate rock. *Miner. Metall. Eng.* **2012**, *32*, 357–361. [[CrossRef](#)]
28. He, B.H.; Liu, H.; Duan, K.B.; Li, L. Research progress of phosphorite deposits in Guizhou. *West. Resour.* **2016**, *3*, 25–30. [[CrossRef](#)]
29. Chen, J.Y.; Zhang, J.; Yang, R.D. Mode of occurrence of rare earth elements in phosphorite in Zhijin County, Guizhou Province, China. *Acta Mineral. Sin.* **2010**, *30*, 123–129. [[CrossRef](#)]
30. Ye, Y.; Al-Khaledi, N.; Barker, L.; Darwish, M.S.; El Naggar, A.M.; El-Yahyaoui, A.; Hussein, A.; Hussein, E.S.; Shang, D.; Taha, M.; et al. Uranium resources in China's phosphate rocks—Identifying low-hanging fruits. *IOP Conf. Ser. Earth Environ. Sci.* **2019**, *227*, 052033. [[CrossRef](#)]
31. Wu, X.H.; Han, Z.J.; Cai, J.F.; Xiao, Y.L. *Phosphorites in Guizhou*; Geological Publishing House: Beijing, China, 1999; pp. 24–29.
32. Wu, J.; Huang, R.X.; Zou, Q.X.; Zhang, Y. Rock falls and their prevention in phosphorus mining area of Kaiyang County, Guizhou province. *Chin. J. Geol. Hazard. Control.* **2011**, *3*, 30–35.
33. Wang, H.S. Kaiyang phosphorite deposit geological features and deep part extended prospecting practices in Guizhou Province. *Coal Geol. China* **2017**, *19*, 34–38. [[CrossRef](#)]
34. Tu, Y.Q. An Environment geological impact on the kaiyang phosphorus district in the central guizhou. *Guizhou Geol.* **1998**, *3*, 273–276.
35. Oliveira, C.M.; Machado, C.M.; Duarte, G.W.; Peterson, M. Beneficiation of pyrite from coal mining. *J. Clean. Prod.* **2016**, *139*, 821–827. [[CrossRef](#)]
36. Sarvamangala, H.; Natarajan, K.A.; Girisha, S.T. Microbially-induced pyrite removal from galena using *Bacillus subtilis*. *Int. J. Miner. Process.* **2013**, *120*, 15–21. [[CrossRef](#)]
37. Dai, S.F.; Ren, D.Y.; Tang, Y.G.; Shao, L.Y.; Li, S.S. Distribution, isotopic variation and origin of sulfur in coals in the Wuda coalfield, Inner Mongolia, China. *Int. J. Coal Geol.* **2002**, *51*, 237–250. [[CrossRef](#)]
38. Dai, S.F.; Ren, D.Y.; Chou, C.L.; Li, S.S.; Jiang, Y.F. Mineralogy and geochemistry of the No. 6 coal (Pennsylvanian) in the Junger Coalfield, Ordos Basin, China. *Int. J. Coal Geol.* **2006**, *66*, 253–270. [[CrossRef](#)]

39. Berner, R.A. Sedimentary pyrite formation: An update. *Geochim. Cosmochim. Acta* **1984**, *48*, 605–615. [[CrossRef](#)]
40. Machel, H.G.; Krouse, H.R.; Sassen, R. Products and distinguishing criteria of bacterial and thermochemical sulfate reduction. *Appl. Geochem.* **1995**, *10*, 373–389. [[CrossRef](#)]
41. Dai, S.; Hou, X.; Ren, D.; Tang, Y. Surface analysis of pyrite in the No.9 coal seam, Wuda Coalfield, Inner Mongolia, China, using high-resolution time-of-flight secondary ion mass-spectrometry. *Int. J. Coal Geol.* **2003**, *55*, 139–150. [[CrossRef](#)]
42. Love, L.G.; Amstutz, G.C. Review of microscopic pyrite from the Devonian Chattanooga Shale and Rammelsberg Banderz. *Fortschr Miner.* **1966**, *43*, 273–309.
43. Wilkin, R.T.; Barnes, H.L.; Brantley, S.L. The size distribution of framboidal pyrite in modern sediments: An indicator of redox conditions. *Geochim. Cosmochim. Acta* **1996**, *60*, 3897–3912. [[CrossRef](#)]
44. Kim, T.B.; Choi, J.W.; Ryu, H.S.; Cho, G.B.; Kim, K.W.; Ahn, J.H.; Cho, K.K.; Ahn, H.J. Electrochemical properties of sodium/pyrite battery at room temperature. *J. Power Sources* **2007**, *174*, 1275–1278. [[CrossRef](#)]
45. Bulut, G.; Yenial, U.; Emiroglu, E.; Sirkeci, A.A. Arsenic removal from aqueous solution using pyrite. *J. Clean. Prod.* **2014**, *84*, 526–532. [[CrossRef](#)]
46. Patra, P.; Natarajan, K.A. Microbially-induced flocculation and flotation for pyrite separation from oxide gangue minerals. *Miner. Eng.* **2003**, *16*, 965–973. [[CrossRef](#)]
47. Shukla, S.; Loc, N.H.; Boix, P.P.; Koh, T.M.; Prabhakar, R.R.; Mulmudi, H.K.; Zhang, J.; Chen, S.; Ng, C.F.; Huan, C.H.A.; et al. Iron pyrite thin film counter electrodes for dyesensitized solar cells: High efficiency for iodine and cobalt redox electrolyte cells. *ACS Nano* **2014**, *8*, 10597–10605. [[CrossRef](#)] [[PubMed](#)]
48. Kraal, P.; Slomp, C.P.; Forster, A.; Kuypers, M.M.M.; Sluijs, A. Pyrite oxidation during sample storage determines phosphorus fractionation in carbonate-poor anoxic sediments. *Geochim. Cosmochim. Acta* **2009**, *73*, 3277–3290. [[CrossRef](#)]
49. Mohapatra, B.K.; Jena, S.; Mahanta, K.; Mishra, P. Goethite morphology and composition in banded iron formation, Orissa, India. *Resour. Geol.* **2008**, *58*, 325–332. [[CrossRef](#)]
50. Jang, K.; Nunna, V.R.M.; Hapugoda, S.; Nguyen, A.V.; Bruckard, W.J. Chemical and mineral transformation of a low grade goethite ore by dehydroxylation, reduction roasting and magnetic separation. *Min. Eng.* **2014**, *60*, 14–22. [[CrossRef](#)]
51. Ravisankar, V.; Venugopal, R.; Bhat, H. Investigation on beneficiation of goethite-rich iron ores using reduction roasting followed by magnetic separation. *Miner. Process. Extr. Metall. Imm Transactions* **2017**, 1–8. [[CrossRef](#)]
52. Li, C.; Sun, H.; Bai, J.; Li, L. Innovative methodology for comprehensive utilization of iron ore tailings: Part 1. The recovery of iron from iron ore tailings using magnetic separation after magnetizing roasting. *J. Hazard. Mater.* **2010**, *174*, 71–77. [[CrossRef](#)]
53. Li, C.; Sun, H.; Yi, Z.; Li, L. Innovative methodology for comprehensive utilization of iron ore tailings: Part 2: The residues after iron recovery from iron ore tailings to prepare cementitious material. *J. Hazard. Mater.* **2010**, *174*, 78–83. [[CrossRef](#)]
54. Fisher-White, M.J.; Lovel, R.R.; Sparrow, G.J. Phosphorus removal from goethitic iron ore with a low temperature heat treatment and a caustic leach. *ISIJ Int.* **2012**, *52*, 797–803. [[CrossRef](#)]
55. Ionkov, K.; Gomes, O.; Neumann, R.; Gaydardzhiev, S.; Correa de Araujo, A. Process oriented characterisation of oolitic iron concentrate during dephosphorisation by roasting and leaching. In Proceedings of the XXVIII International Mineral Processing Congress (IMPC 2016), West Westmount, QC, Canada, 10–15 September 2016.
56. Kokal, H.R.; Singh, M.P.; Naydyonov, V.A. *Removal of Phosphorus from Lisakovsky Iron Ore by a Roast Leach Process*; John Wiley and Sons, Inc.: New York, NY, USA, 2003; pp. 1517–1530.
57. Zhang, L.; Machiela, R.; Das, P.; Zhang, M.M.; Eisele, T. Dephosphorization of unroasted oolitic ores through alkaline leaching at low temperature. *Hydrometallurgy* **2018**, *184*, 95–102. [[CrossRef](#)]
58. Zhang, L.; Ankathi, S.K.; Zhang, M.M.; Eisele, T.C. Bio-extraction of phosphorus from goethite ore with alkali addition. *Miner. Eng.* **2019**, *141*, 105850. [[CrossRef](#)]
59. Yellishetty, M.; Ranjith, P.G.; Tharumarajah, A. Iron ore and steel production trends and material flows in the world: Is this really sustainable? *Resour. Conserv. Recycl.* **2010**, *54*, 1084–1094. [[CrossRef](#)]
60. Williams, P.J. The use of *Aspergillus niger* for the Removal of Potassium and Phosphorous from the Iron Ore of the Sishen Iron Ore Mine, South Africa. Ph.D. Thesis, University of Pretoria, Pretoria, South Africa, 2008.

61. Ndlovu, B.; Becker, M.; Forbes, E.; Deglon, D.; Franzidis, J.P. The influence of phyllosilicate mineralogy on the rheology of mineral slurries. *Miner. Eng.* **2011**, *24*, 1314–1322. [[CrossRef](#)]
62. Bracke, G.; Satir, M.; Krau, P. The cryptand (222) for exchanging cations of micas. *Clay Clay Miner.* **1995**, *43*, 732–737. [[CrossRef](#)]
63. Bubnova, T.; Skamnitskaya, L.; Gorbunova, E.; Chertov, A. Contrast characteristics of the muscovitic quartzite from Karelia, Russia—Determining the possibility of intensification of the beneficiation process. *IOP Conf. Ser. Earth Environ. Sci.* **2017**, *95*, 042072. [[CrossRef](#)]

**Publisher’s Note:** MDPI stays neutral with regard to jurisdictional claims in published maps and institutional affiliations.



© 2020 by the authors. Licensee MDPI, Basel, Switzerland. This article is an open access article distributed under the terms and conditions of the Creative Commons Attribution (CC BY) license (<http://creativecommons.org/licenses/by/4.0/>).